

Phosphorescent Bio-Based Resin for Digital Light Processing (DLP) 3D-Printing

Mirko Maturi, Carolina Pulignani, Erica Locatelli, Veronica Vetri Buratti, Letizia Sambri, Mauro Comes Franchini**

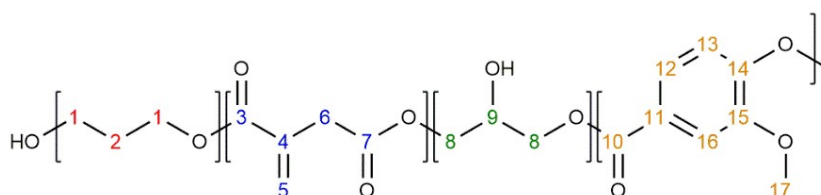
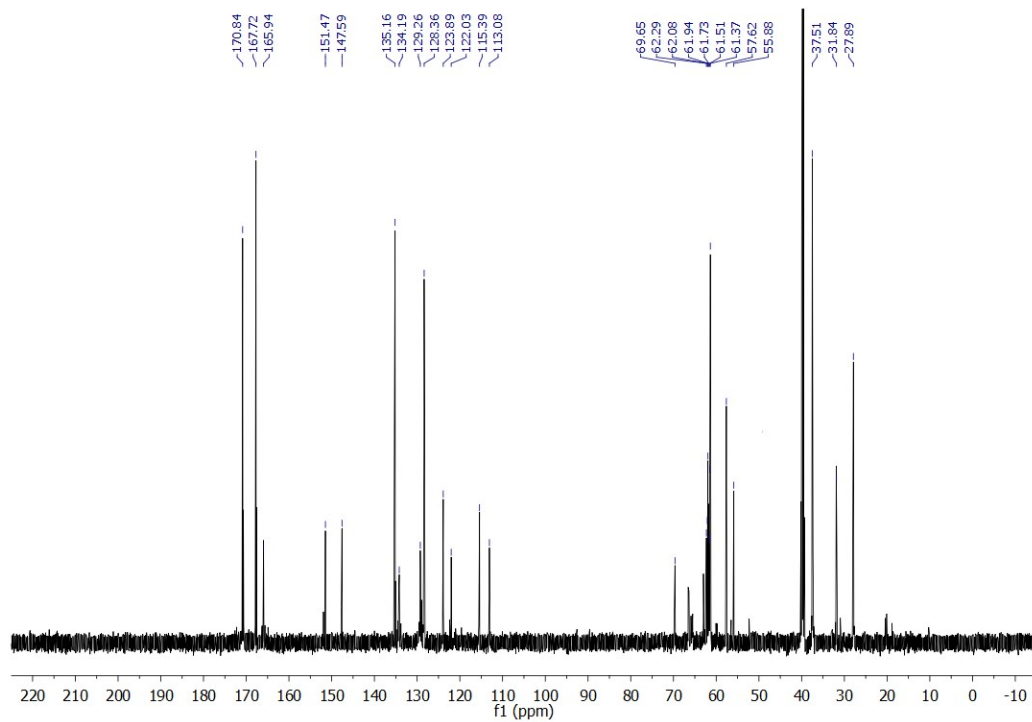
Department of Industrial Chemistry “Toso Montanari”, University of Bologna
Viale Risorgimento 4, 40136 Bologna, Italy
E-mail: mauro.comesfranchini@unibo.it, letizia.sambri@unibo.it

SUPPORTING INFORMATION

TABLE OF CONTENTS

NMR ANALYSIS.....	2-4
3D PRINTED MODELS.....	5
PHOTOCURABLE POLYESTER – EXPLORED BIOBASED MONOMERS.....	6
PHOTOCURABLE POLYESTER – COMPOSITIONAL ANALYSIS.....	7
MECHANICAL TESTS – TENSILE TEST.....	9
MECHANICAL TESTS – FLEXURAL TEST.....	10
ATR-FTIR ANALYSIS.....	11
ELECTRON MICROSCOPY (SEM).....	12
THERMAL ANALYSES.....	13
PHOSPHORIMETRIC STUDIES.....	14-17
EFFECT OF VANILLIC ACID ON PRINTABILITY.....	18
BIOCOMPATIBILITY TESTS.....	19-20

NMR ANALYSIS



Carbon #	Chemical Shift (ppm)
3	170.84
4	135.16 – 134.19
5	129.26 – 128.36
6	37.51
7	167.72
2	31.84 – 27.89
1	69.65 – 65.25 – 62.29 –
8	62.08 – 61.94 – 61.73 –
9	61.51 – 61.37 – 57.62

Carbon #	Chemical Shift (ppm)
10	165.94
11	122.03
12	123.89
13	113.08
14	151.47
15	147.59
16	115.39
17	55.88

Figure S1 - ^{13}C -NMR (150 MHz, $\text{DMSO-}d_6$) of PPGIV, and corresponding peak assignment. Some of the carbon atoms can be related to multiple peaks due to the presence of terminal and non-terminal monomers in comparable concentrations.

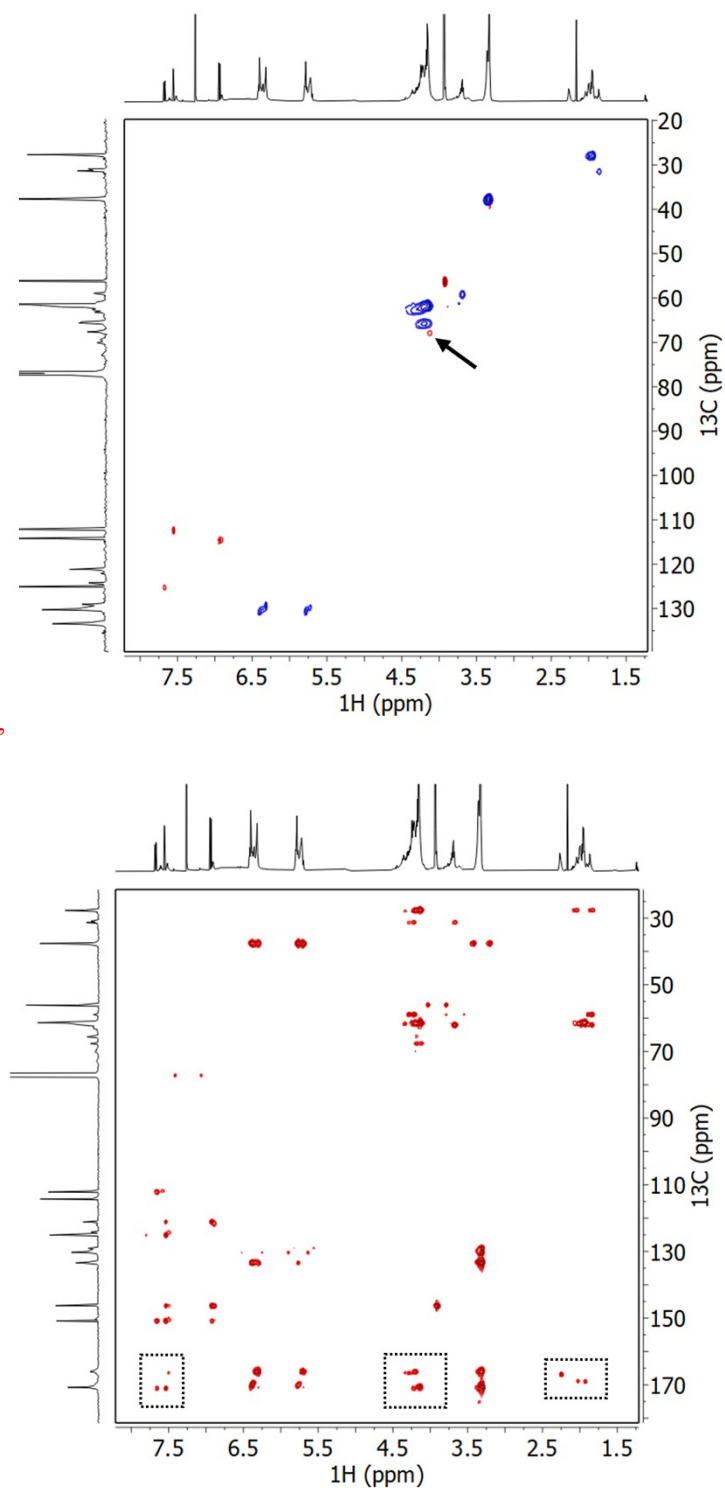


Figure S2 - ^1H - ^{13}C gHSQC (top) and gHMBC (bottom) NMR spectra (600 MHz, CDCl_3) of PPGIV. Since gHSQC experiment is phase-sensitive, it allows to distinguish between CH + CH_3 (red cross peaks) and CH_2 groups (blue cross peaks). The cross peak pointed with the arrow corresponds to CH residues on branched glycerol units, confirming that with the employed polymerization conditions glycerol is able to form branched structures. However, the analogous cross peak corresponding to linear or terminal glycerol units is most probably overlapped with the other polyols signals (in the region between 60-70 ppm for ^{13}C and 3.5-4.5 ppm for ^1H). The gHMBC spectrum displays ^1H - ^{13}C correlations at longer distance than gHSQC, allowing to observe some inter-monomer correlations (cross peaks in dotted boxes).

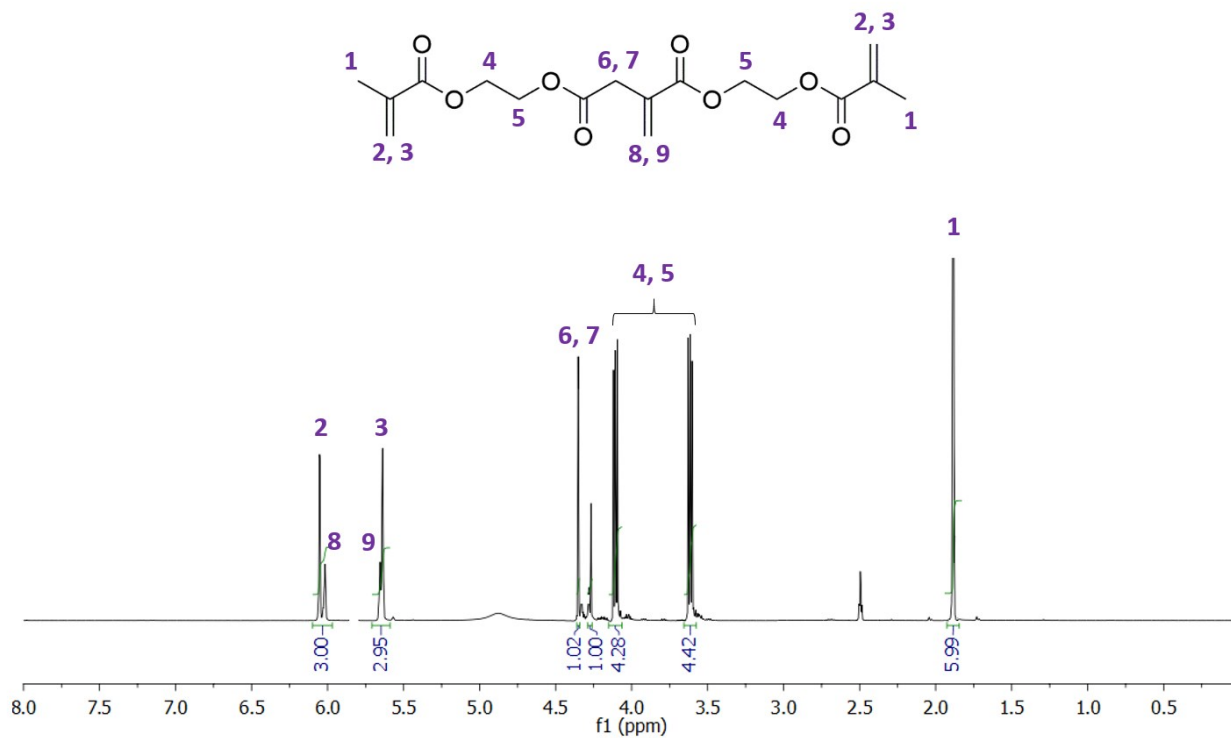


Figure S3 - ¹H-NMR (400 MHz, DMSO-*d*₆) of BHI.

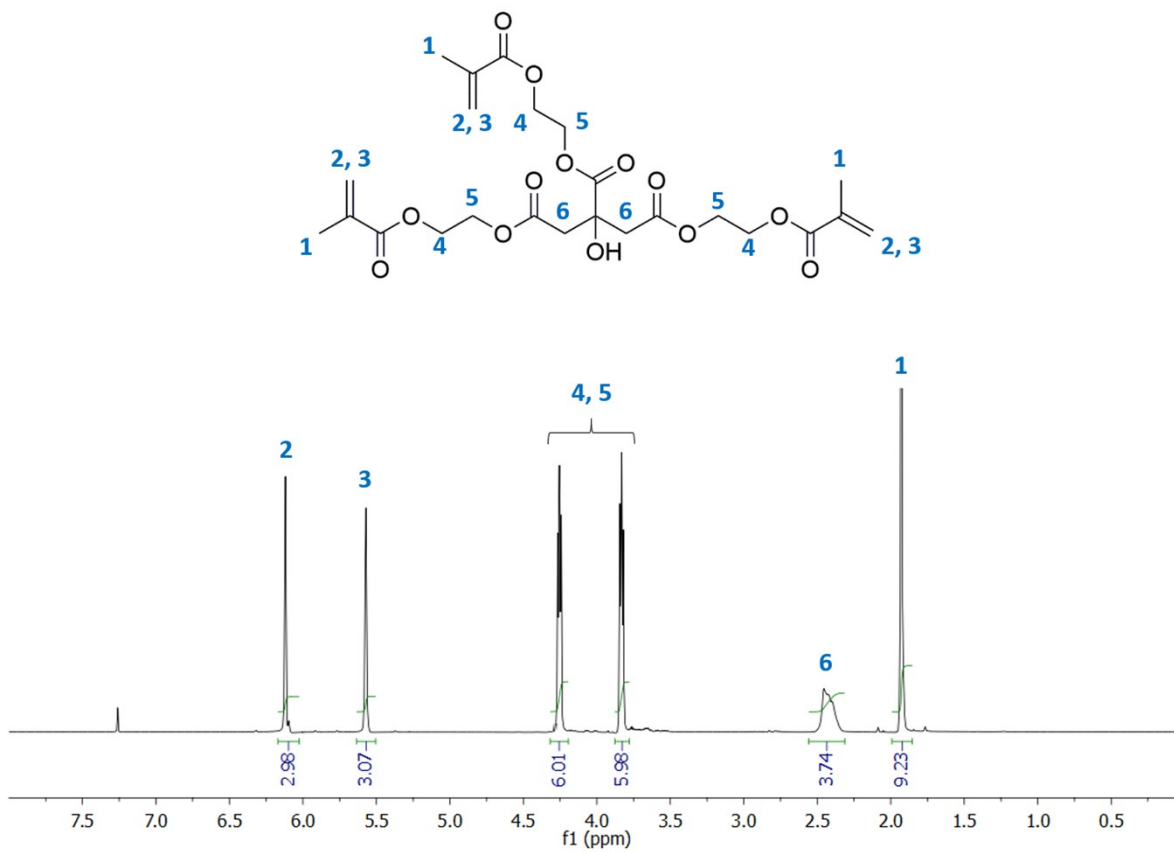


Figure S4- ¹H-NMR (400 MHz, CDCl₃) of THC.

3D PRINTED MODELS

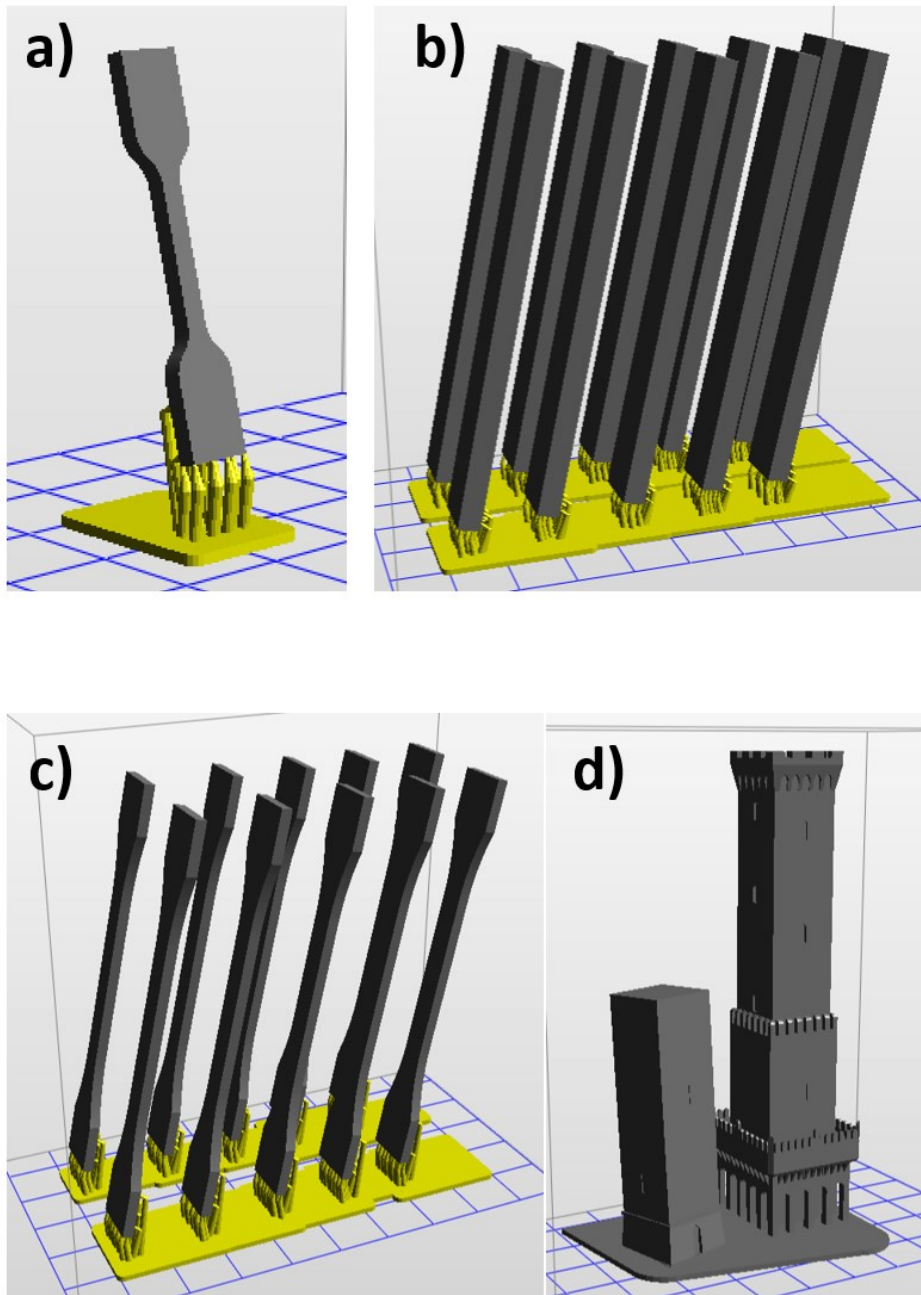


Figure S5 - Post-design processing of the 3D printed models, with the supports required for structural stability during the printing process. a) Small dog-bone for ink tests and phosphorimetric studies (6x1.8x35 mm). Total printing time: 2 h 35 min; b) bars for flexural and impact tests (80x10x4 mm). Total printing time: 8 h 15 min; c) Dog-bones for tensile tests (ISO-527-1BA, 77x10x2 mm). Total printing time: 7 h 20 min; d) Model for the historical towers “Le Due Torri” of the city of Bologna, Italy. Total printing time: 12 h 55 min.

PHOTOCURABLE POLYESTER – EXPLORED BIOBASED MONOMERS

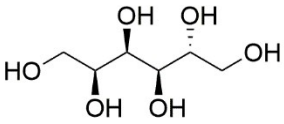
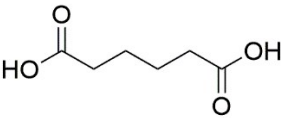
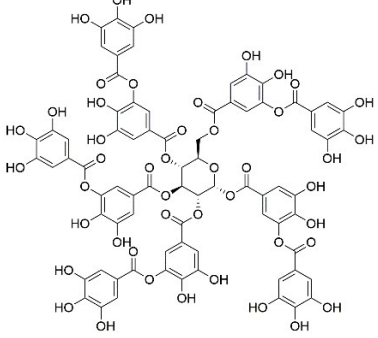
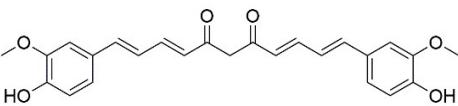
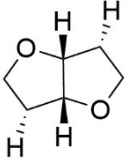
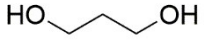
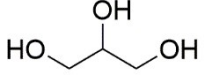
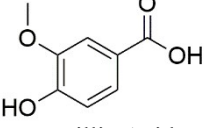
MONOMER	PROS	CONS
 <p>Sorbitol</p>	Green monomer obtained by reduction of glucose. Low cost	Due to increased branching, the polyester was vitreous and not suitable for the application
 <p>Adipic Acid</p>	Biobased and hydrophobic	It reduces the amount of itaconic acid entrapped in the polyester, hindering its photocuring
 <p>Tannic Acid</p>	Naturally occurring polyphenol, employed in food industry and as medication.	The high temperature polyesterification causes the formation of polyphenols, making the polyester black and insoluble
 <p>Curcumin</p>	Naturally occurring. Forms yellow-orange polymers, capable of green fluorescence	Hard to purify. Curcumin is only soluble in organic solvents and alkaline water, and curcumin-containing polyesters reflected its solubility
 <p>Isosorbide</p>	Obtained by dehydration of sorbitol through sorbitan.	High cost. Highly hydroscopic, which reduced the polyesterification efficiency due to the presence of moisture. Probable degradation at the reaction condition, causing the formation of orange-to-brown polyesters.
 <p>1,3-propanediol</p>	Low cost. Green synthesis processes already at the industrial scale.	NONE OBSERVED
 <p>Glycerol</p>	Low cost. Side product of the production of biodiesel.	NONE OBSERVED
 <p>Vanillic Acid</p>	Naturally occurring, produced by air oxidation of vanillin.	NONE OBSERVED

Table S1 – Explored biobased monomers for the production of photocurable polyester to be employed for DLP 3D printing, together with the pros for which they have been chosen and the cons for which they have been discarded.

PHOTOCURABLE POLYESTER – COMPOSITIONAL ANALYSIS

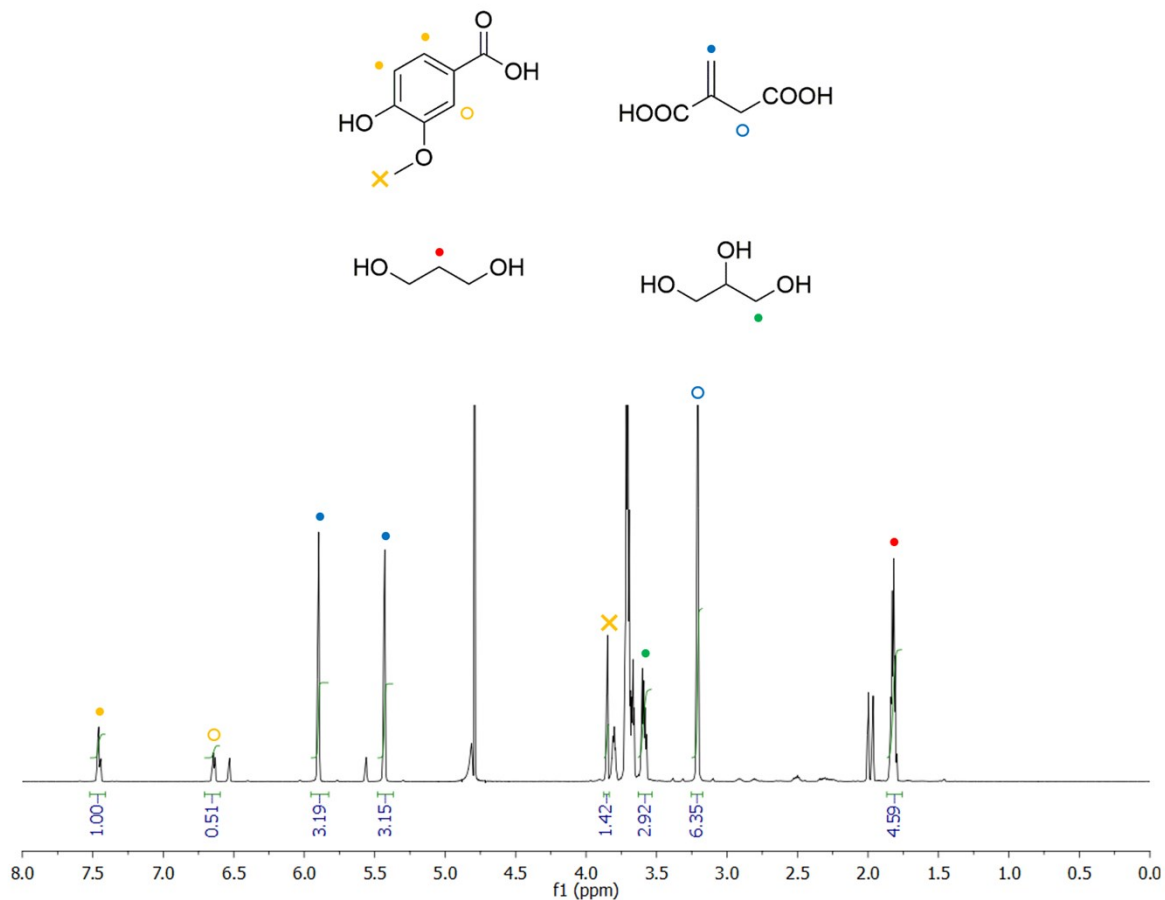


Figure S6 - $^1\text{H-NMR}$ (600 MHz, $\text{D}_2\text{O}/\text{H}_2\text{O}$ 1:1) – Solvent signal suppression pulse of PPGIV after hydrolysis. Unambiguously assignable peaks have been integrated in order to establish the molar composition of the prepared oligomer.

In order to get the molar ratio between monomers, first of all each signal integral has been divided by the number of protons it represents, and signals from the same monomers have been averaged. As a general formula:

$$n_x = \frac{1}{k_x} \sum_{m=1}^k \frac{\int S_m(x)}{N_{S_m(x)}}$$

Where n_x is proportional to the number of moles of monomer x , k_x is the number of signals that can be attributed to monomer x , $\int S_m(x)$ is the integral of the m^{th} NMR signal of monomer x and $N_{S_m(x)}$ is the number of protons represented by the m^{th} NMR signal of monomer x .

Therefore:

$$\begin{aligned}
 n_{Vanillic} &= \frac{1}{3} \left[\frac{1.00}{2} + \frac{0.51}{1} + \frac{1.42}{3} \right] = 0.49 \\
 n_{Itaconic} &= \frac{1}{3} \left[\frac{3.19}{1} + \frac{3.15}{1} + \frac{6.35}{2} \right] = 3.17 \\
 n_{PDO} &= \frac{4.59}{2} = 2.30 \\
 n_{Glycerol} &= \frac{2.92}{2} = 1.46
 \end{aligned}
 \left. \vphantom{\begin{aligned} n_{Vanillic} \\ n_{Itaconic} \\ n_{PDO} \\ n_{Glycerol} \end{aligned}} \right\} n_{Total} = \sum n_x = 7.42$$

And the molar ratios calculated accordingly:

$$x_{Vanillic} = 1.0$$

$$x_{Itaconic} = 6.5$$

$$x_{PDO} = 4.7$$

$$x_{Glycerol} = 3.0$$

Then, the weight composition has been obtained by using the same approach, but multiplying each n_x by the corresponding molecular weight:

$$\begin{aligned}
 m_{Vanillic} &= n_{Vanillic} \cdot MW_{Vanillic} = 0.49 \cdot 168.14 = 82.4 \\
 m_{Itaconic} &= n_{Itaconic} \cdot MW_{Itaconic} = 3.17 \cdot 130.1 = 412 \\
 m_{PDO} &= n_{PDO} \cdot MW_{PDO} = 2.30 \cdot 76.09 = 175 \\
 m_{Glycerol} &= n_{Glycerol} \cdot MW_{Glycerol} = 1.46 \cdot 92.09 = 134
 \end{aligned}
 \left. \vphantom{\begin{aligned} m_{Vanillic} \\ m_{Itaconic} \\ m_{PDO} \\ m_{Glycerol} \end{aligned}} \right\} m_{Total} = \sum m_x = 803.4$$

And the weight percentages calculated accordingly:

$$x_{Vanillic} = 10 \text{ wt\%}$$

$$x_{Itaconic} = 51 \text{ wt\%}$$

$$x_{PDO} = 22 \text{ wt\%}$$

$$x_{Glycerol} = 17 \text{ wt\%}$$

MECHANICAL TESTS – TENSILE TEST

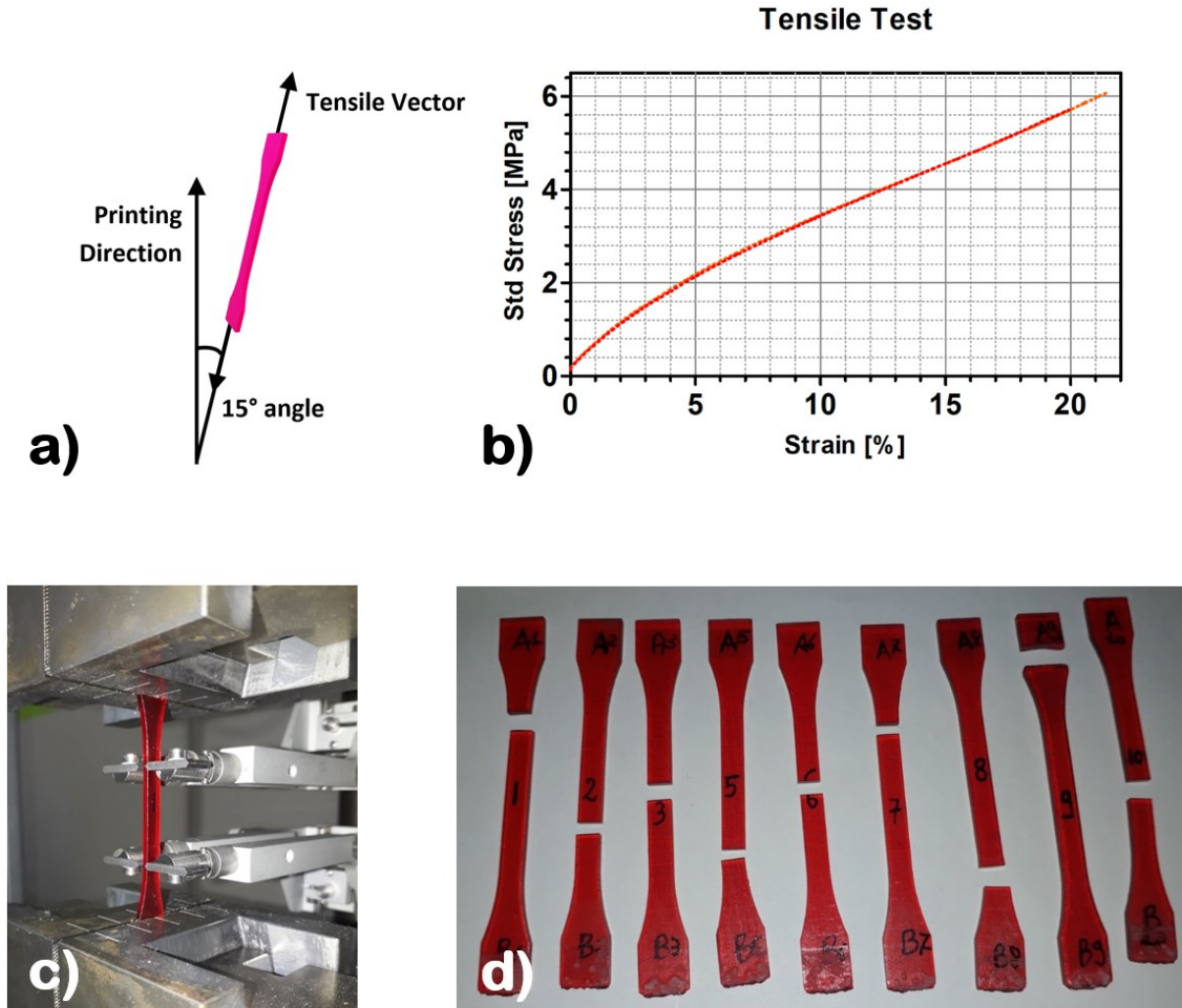


Figure S7 - Tensile tests. a) Schematic representation of the direction of the tensile test with respect to the direction of the 3D printing process. b) Stress-strain plot. c) Picture of the experimental setup. d) Picture of the broken dog-bones, showing that the breaking point is randomly distributed throughout the different experiments.

MECHANICAL TESTS – FLEXURAL TEST

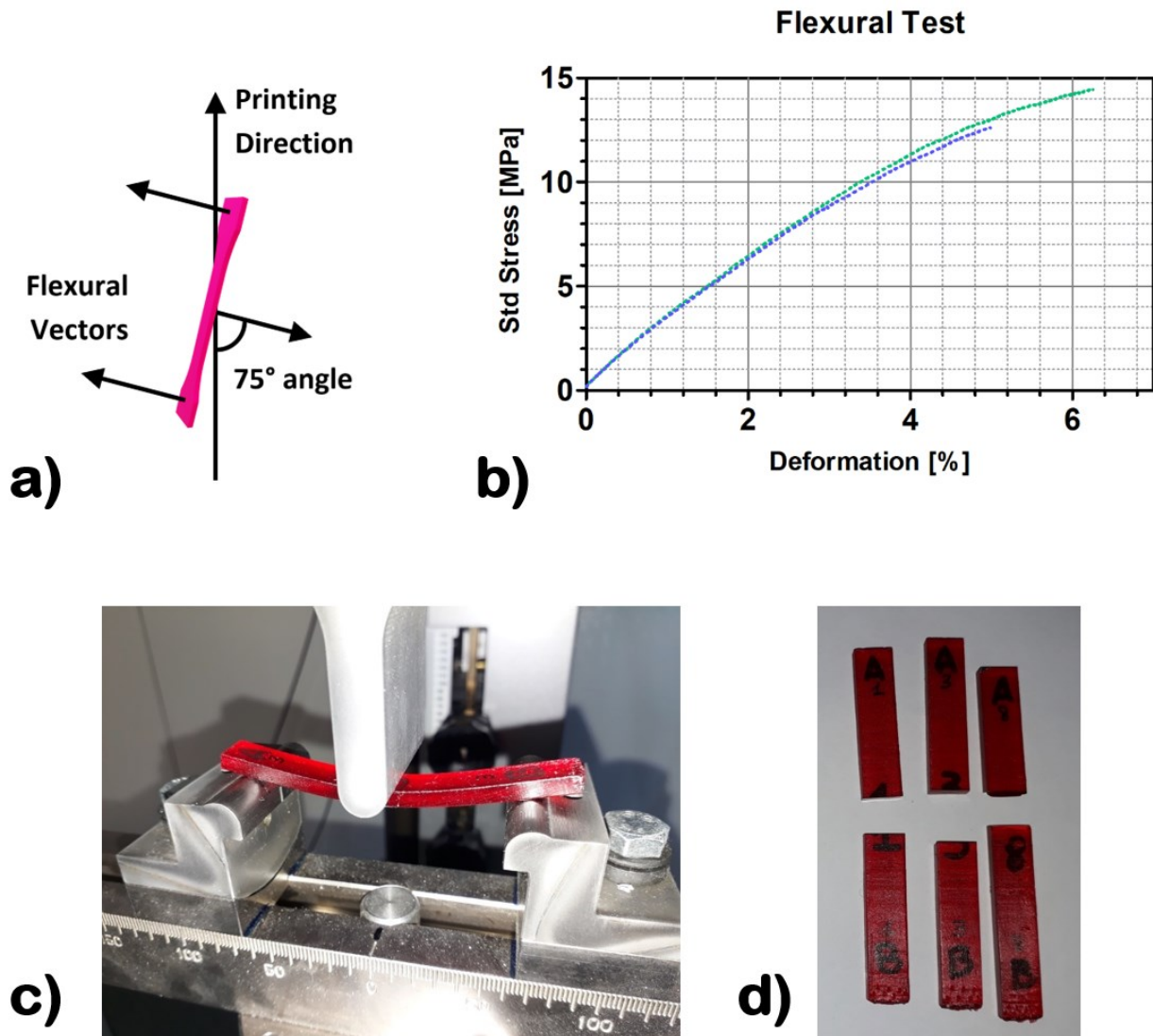


Figure S8 - Flexural tests. a) Schematic representation of the directions of the flexural test with respect to the direction of the 3D printing process. b) Stress-deformation plot. c) Picture of the experimental setup. d) Picture of the broken test bars.

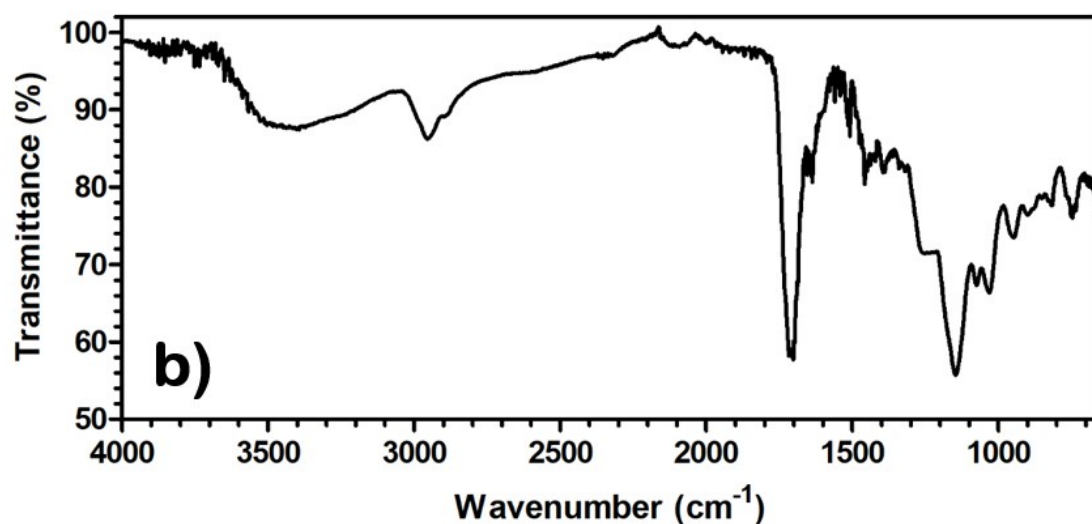
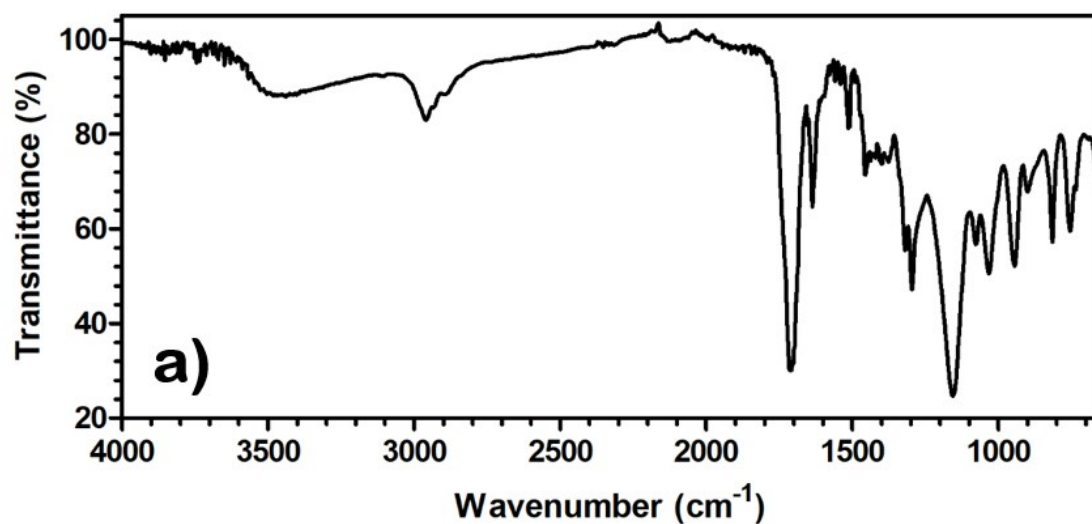


Figure S9 - ATR-FTIR analysis on the photocurable ink before (a) and after (b) the 3D printing process.

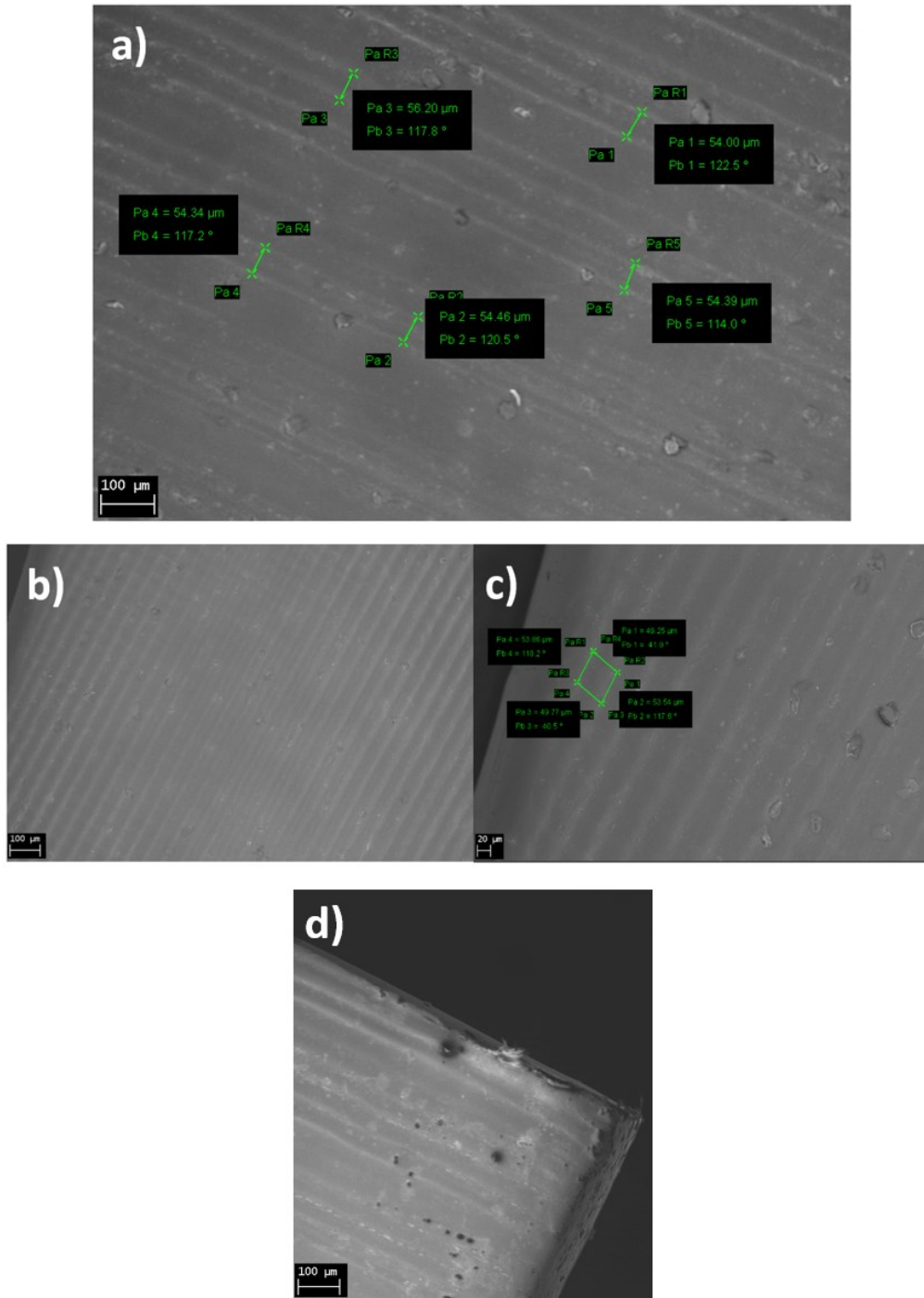


Figure S10 - Morphology of the 3D printed material explored by SEM. a) Lateral view of the printed object, which allows to measure the distance between printed layers. b,c) Top view of the irradiated slice, which allows to distinguish projected squared pixels and to measure their size. d) Details of an edge of the printed structure.

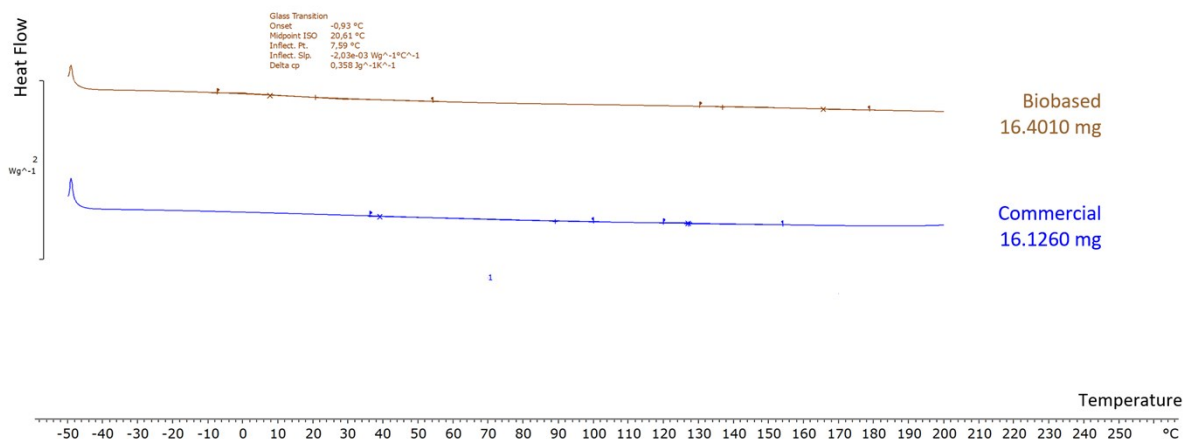


Figure S11 - Comparison of DSC traces of photopolymerized commercial and biobased inks. The curve related to the material printed with the developed biobased ink display a small endothermic process occurring at around 7.6°C, which can be attributed to a glass transition of PPGIV.

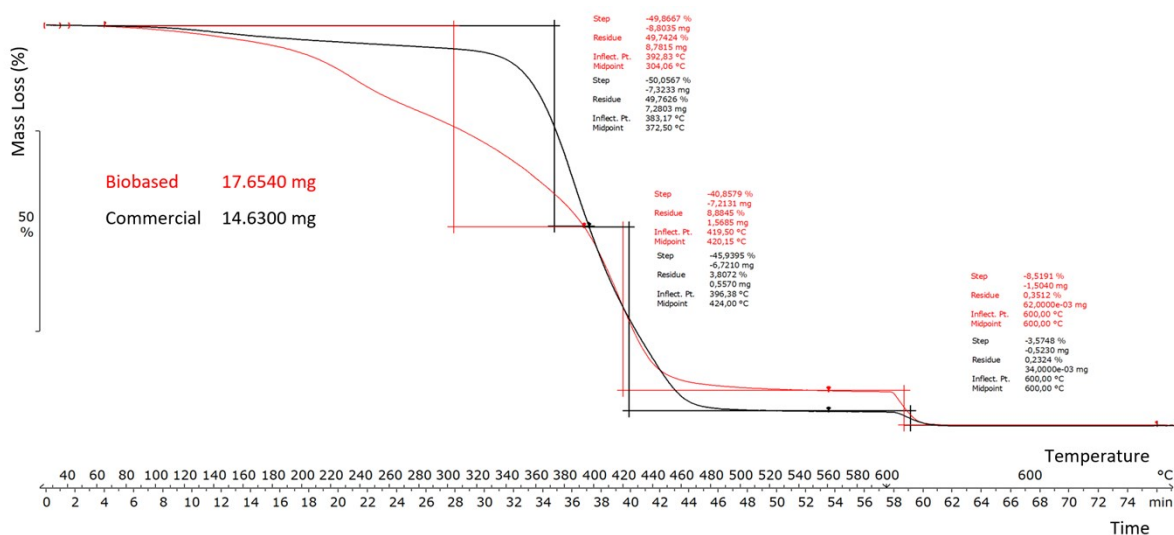


Figure S12 - Comparison of TGA analyses performed on photopolymerized commercial and biobased inks. The developed biobased ink display lower temperature stability compared to the commercial counterpart but comparable residual mass after complete calcination.

1) Blue Ink

DYE = Unisol Blue AS

COMPLEX = $[\text{Ir}(\text{dfppy})_2(\text{b-trz})]^- \text{K}^+$

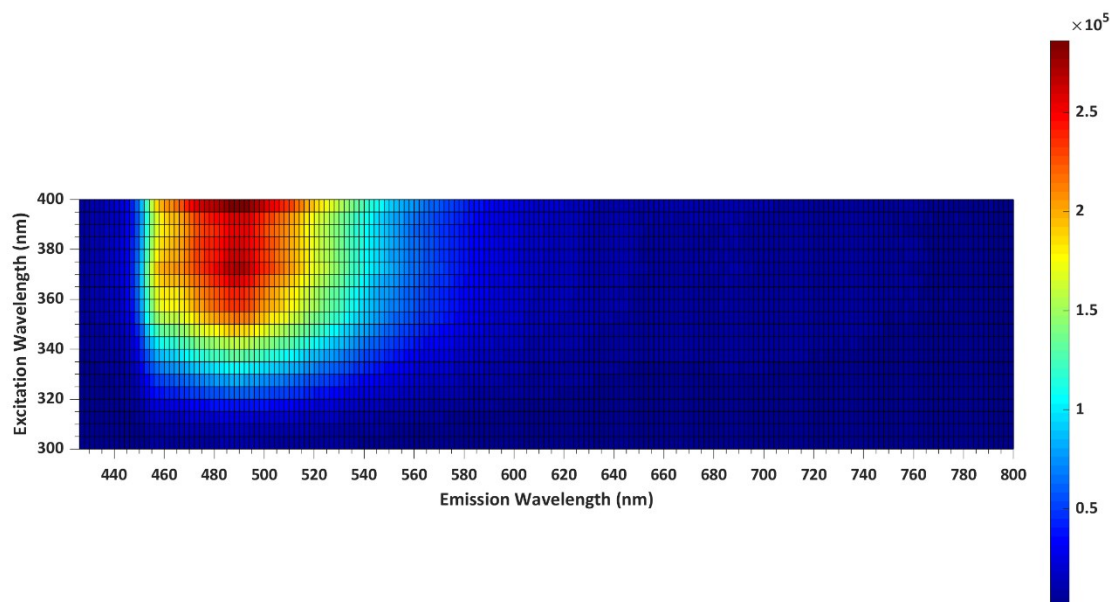
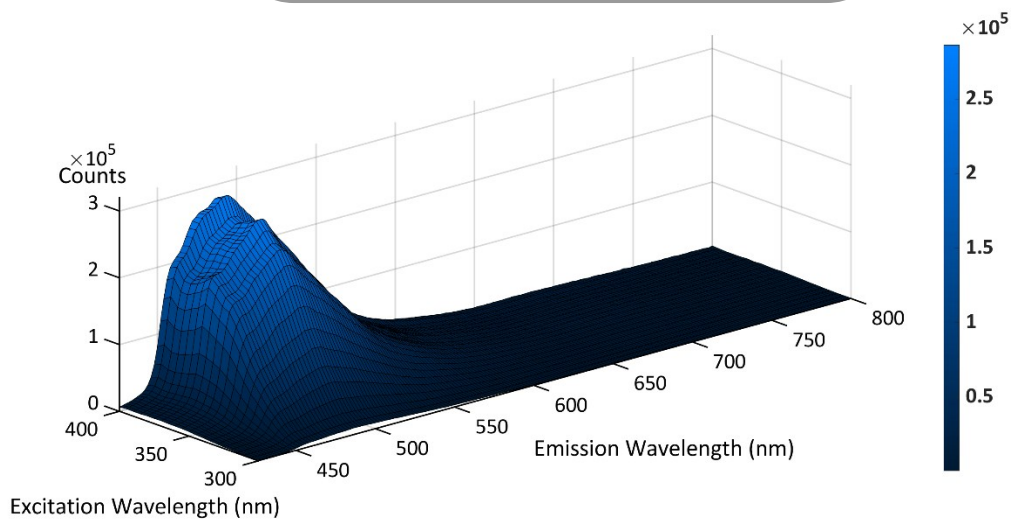
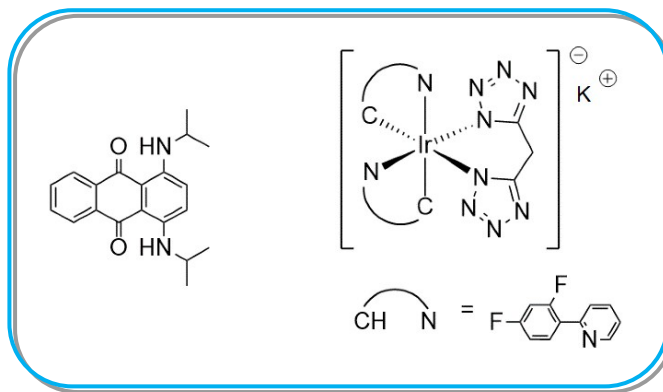


Figure S13 - Emission maps of the 3D printed blue phosphorescent ink (small dog-bone, top, left). The same emission data are represented with a 3D surface plot (top, right) and with a color-scale 2D image plot (bottom). Color scale bars represent counts of the photodetector.

2) Green Ink

DYE = Solvent Green 3

COMPLEX = $[\text{Ir}(\text{ppy})_2(\text{b-trz})]^- \text{K}^+$

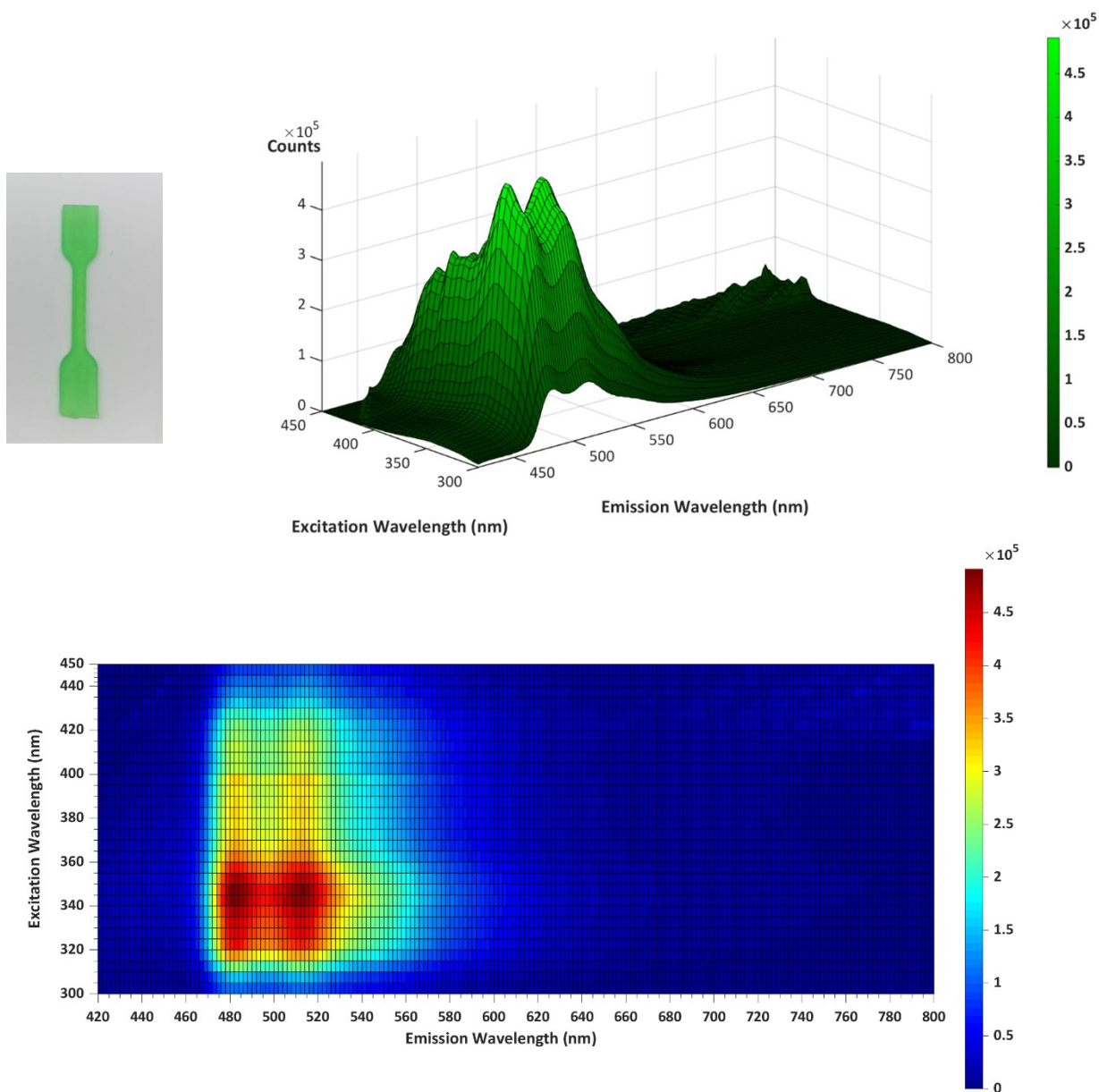
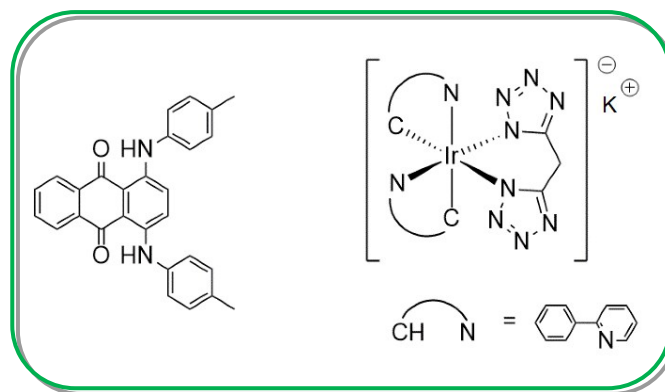


Figure S14 – Emission maps of the 3D printed green phosphorescent ink (small dog-bone, top, left). The same emission data are represented with a 3D surface plot (top, right) and with a color-scale 2D image plot (bottom). Colour scale bars represent counts of the photodetector.

3) Yellow Ink

DYE = Cresol Red

COMPLEX = $[\text{Ir}(\text{ppy})_2(\text{bpy})]^+ \text{Cl}^-$

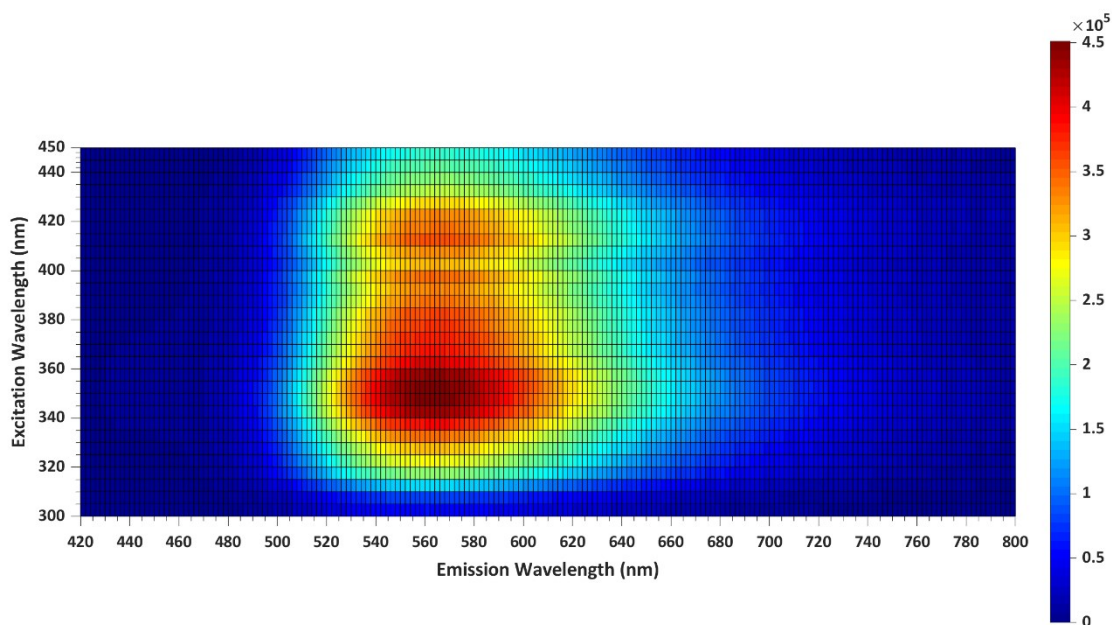
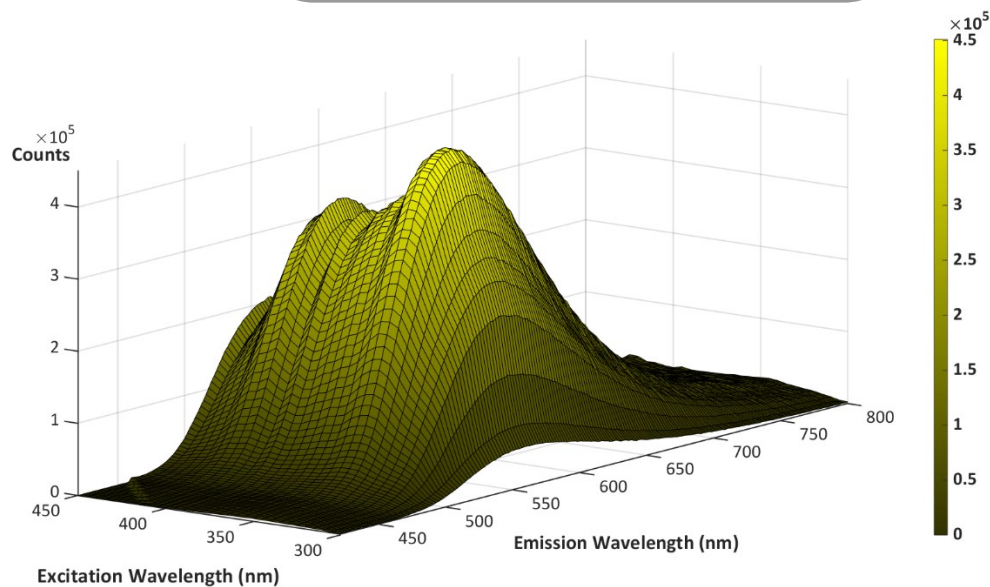
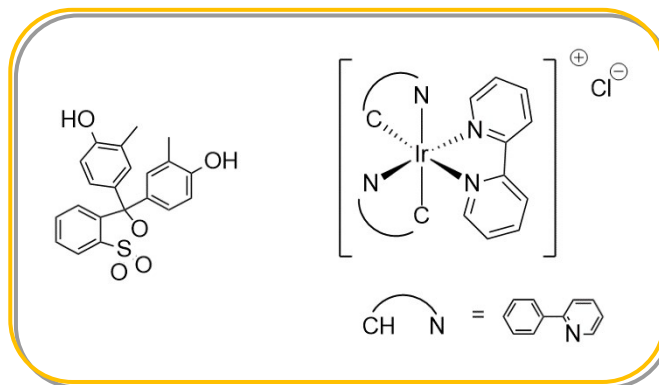


Figure S15 – Emission maps of the 3D printed yellow phosphorescent ink (small dog-bone, top, left). The same emission data are represented with a 3D surface plot (top, right) and with a color-scale 2D image plot (bottom). Colour scale bars represent counts of the photodetector.

4) Red Ink

DYE = Methyl Red

COMPLEX = $[\text{Ir}(\text{pqu})_2(\text{b-trz})]^- \text{TBA}^+$

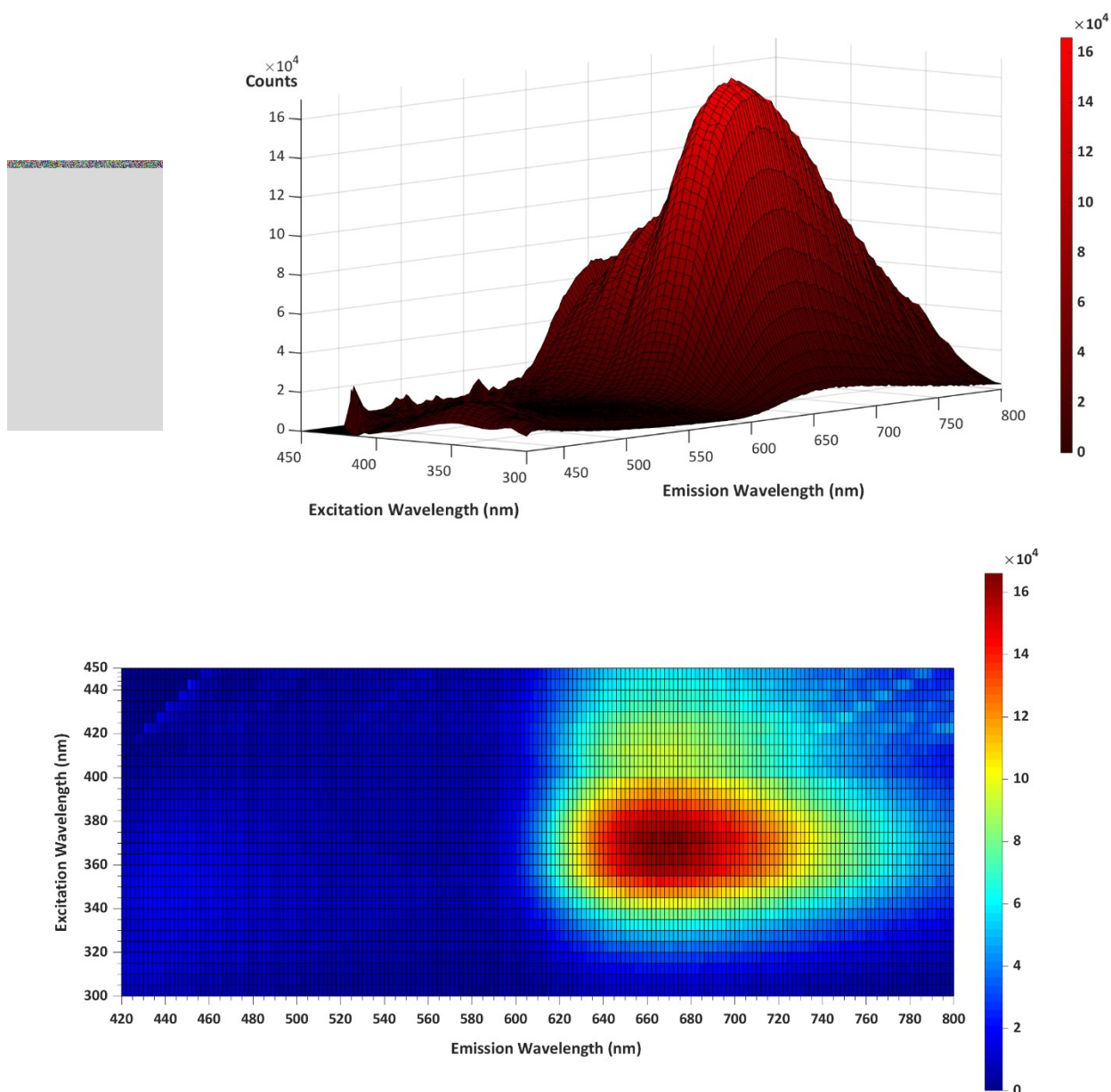
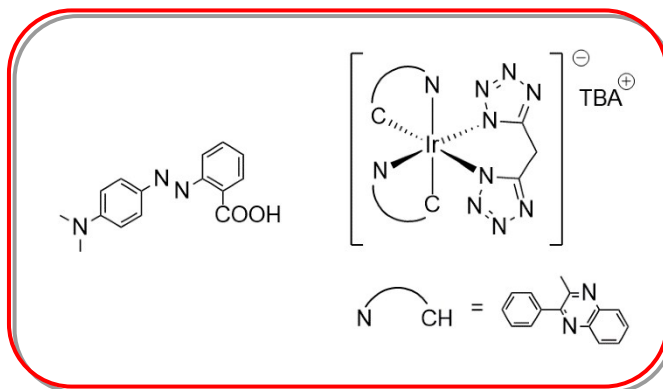


Figure S16 - Emission maps of the 3D printed red phosphorescent ink (small dog-bone, top, left). The same emission data are represented with a 3D surface plot (top, right) and with a colour-scale 2D image plot (bottom). Colour scale bars represent counts of the photodetector.

EFFECT OF VANILLIC ACID ON PRINTABILITY

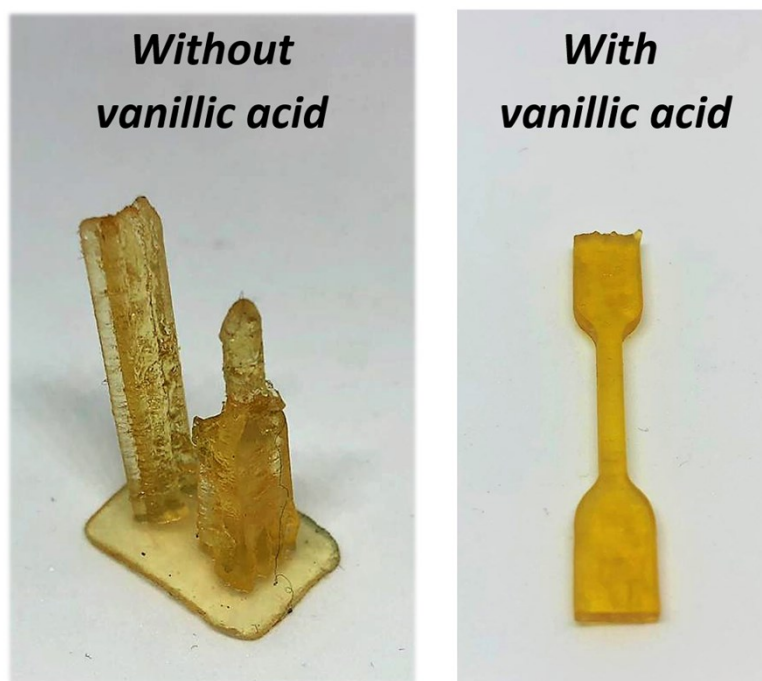


Figure S17 – Effect of vanillic acid on the 3D printing properties of the photocurable polyester. In the absence of vanillic acid, resolution is very low leading to blurred edges, and the printed object generally breaks.

BIOCOMPATIBILITY TESTS

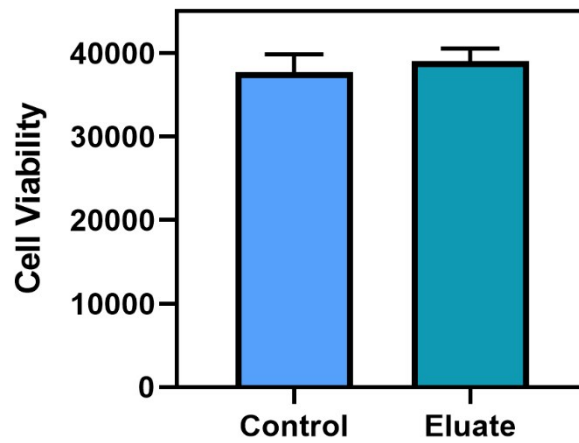
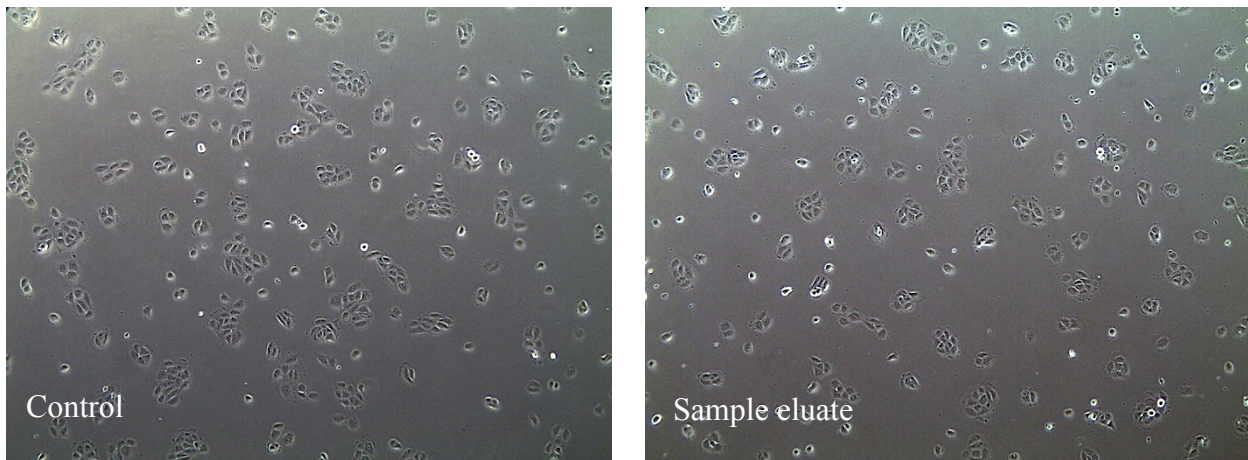


Figure S18 – HaCaT cell viability test. HaCaT cells seeded on multiwell 6 polystyrene plate with and without exposure to the printed sample eluate: the control (on the left) and the treated (on the right) show no difference in cell morphology (optical microscope image above) and the 24h count displays how even if in presence of the eluate, cell viability is not adversely affected.

In Vitro Analysis of the Pro-Sensitising Potential

	Value	Limits	Results
PI (for all the samples)	>80%	>80%	Complies
MFI positive control (lower concentration compared to negative control)	+28.71% CD54 +28.49% CD86	>10%	Complies

Table S2 – Assay validity requirements. Acceptance criteria of the assay comply; hence the assay is valid.

Sample	CD54		CD86		PI
	MFI	% compared to negative control	MFI	% compared to negative control	
Nickel Sulfate 20 µg/ml	50.87	107.46	102.56	408.98	86
Nickel Sulfate 10 µg/ml	40.12	63.32	52.45	160.30	86
Nickel Sulfate 4 µg/ml	31.56	28.71	25.89	28.49	87
3D Printed Material (eluate, 100 µl/ml)	24.19	-1.35	20.05	-0.50	88
3D Printed Material (eluate, 20 µl/ml)	24.18	-1.39	20.08	-0.35	87
Negative control	24.52		20.15		87
MFI CUT OFF	25.21		20.66		

Table S3 – FACS results of CD54 and CD86 expression reported as MFI values. MFI is the geometric mean of the fluorescence intensity of the cells decorated with the fluoresceinated antibody, MFI is proportional to the number of stained molecules per cell. The MFI values are considered significantly increased as a result of incubation with the test product, when they are higher than the value of "MFI cut-off" that is obtained by increasing the MFI of the negative control by defined percentage value. The latter is obtained by dividing the mean + 2 standard deviations of a series of 10 determinations of MFI performed on as 10 negative control samples for the value of the MFI of the negative control itself. This determination is carried out every six months as a measure of intra-assay variability.